electronics

MDPI

Article

Multi-Objective Optimal Scheduling of a Hybrid Ferry with Shore-to-Ship Power Supply Considering Energy Storage Degradation

Kyaw Hein [1,*], Xu Yan [1,*] and Gary Wilson [2]

[1] School of Electrical and Electronic Engineering, Nanyang Technological University, Singapore 639798, Singapore

[2] Rolls-Royce Electrical, Rolls-Royce, Singapore 639798, Singapore; gary.wilson5@Rolls-Royce.com

* Correspondence: hein@live.com.sg (K.H.); eeyanxu@gmail.com (X.Y.)

Received: 29 April 2020; Accepted: 19 May 2020; Published: 20 May 2020

Abstract: To improve the operation efficiency and reduce the emission of a solar power integrated hybrid ferry with shore-to-ship (S2S) power supply, a two-stage multi-objective optimal operation scheduling method is proposed. It aims to optimize the two conflicting objectives, operation cost (fuel cost of diesel generators (DGs), carbon dioxide (CO_2) emission tax and S2S power exchange) and energy storage (ES/ESS) degradation cost, based on the preference of the vessel operator and solar photovoltaic (PV) power output. For the day-ahead optimization, interval forecast data of the PV is used to map the solution space of the objectives with different sets of weight assignment. The solution space from the day-ahead optimization is used as a guide to determine the operating point of the hour-ahead optimization. As for the hour-ahead scheduling, more accurate short-lead time forecast data is used for the optimal operation scheduling. A detailed case study is carried out and the result indicates the operation flexibility improvement of the hybrid vessel. The case study also provides more in-depth information on the dispatching scheme and it is especially important if there are conflicting objectives in the optimization model.

Keywords: energy storage; electric ship charging; generation scheduling; hybrid electric ferry; multi-objective optimization; operation scheduling; renewable energy sources; shore-to-ship power

1. Introduction

In 2008, more than 90% of global trading was carried out by maritime transportation and it is expected to be tripled by 2025. The international maritime organization (IMO) stated that if no necessary actions are taken to improve the energy efficiency of the vessel, carbon dioxide (CO_2) emission will increase by 250% by the end of 2050 [1]. Emission at the harbor area has greater influences on the onshore environment and hence the operation of vessels near shore becomes the major concern for the marine industry [2–4]. The emission level of the ships is restricted by the authorities and some of the on-board diesel generators (DGs) are forced to switch off when the vessel is approaching the harbor. Improvement measures such as renewable energy source (RES), energy storage system (ESS) and shore-to-ship (S2S) power supply integration, are proposed by regulatory authorities, and many literatures [5–26] have pointed out the applicability of such technologies on ship power system operation. The proposed technologies introduce additional flexibility, as well as complexity in the system operation scheduling, and hence should be thoroughly explored. As a result, the key research challenge is to design an optimal operation scheduling of the more-electric vessel with the consideration of the proposed improvement measures.

2. Literature Review

In [5], the initiatives toward sustainable transport systems with the help of RESs such as PV are highlighted. The findings indicate that RESs can significantly reduce the overall fuel consumption of the transportation network if they are managed efficiently. However, RESs are stochastic in nature and the addition of such energy sources adds complexity to the system optimal operation scheduling. The uncertainty presents in PV power generation can be efficiently addressed by the integration of the ES. ES not only addresses the uncertainty present in the RESs [5,6] but also provides additional dimensions to the optimal operation scheduling of the vessels such as optimal loading of the DGs, peak shaving, energy reserve, and uninterruptible power supply [11,13,14,17–20]. Yet, full battery-powered vessels are still fewer in number due to the limited capacity of the ES for longer voyages. Only a short duration battery-powered or hybrid vessels are tested and developed much more frequently. An extensive simulation study in [21] has demonstrated that ES can reduce the fuel consumption of more-electric ships. The multi-objective nature of the ship power system with ES is further analyzed in [14]. The study has considered cooperating objectives such as fuel consumption minimization and emission reduction. The result indicates that aside from the fuel consumption reduction, ES can also reduce the overall CO_2 emission per transport work. However, such a form of the objective formulation will result in ES to be charged and discharged much more frequently and hence resulting in the accelerated degradation of the ES. Furthermore, the effects of ESS integration on the PV integrated vessels are also analyzed in [15,16,23], and the results indicate that proper deployment of the ES can successfully address the uncertainty present in the PV uncertainty while reducing the overall emission of the vessel. Generally, the S2S power supply system or cold-ironing is used to further curtail the emission at seaport territory while assisting the charging of the ES. The S2S power supply allows some or all the on-board DGs to be switched off while the vessel is at berth. A hybrid DGs/ES vessel can benefit greatly from the S2S power supply [5,6,11]. However, the S2S power supply might use non-renewable resources, and hence economic factors are needed to be considered while designing the operation scheduling of the ship power system for the grid-connected operation mode [12].

In [13,14,17–19], the energy management strategies for the hybrid vessels are presented. Most of them address the emission and fuel cost minimization as their main objective in the optimization problem. However, these two objectives encourage the heavy reliance on the ES and the renewable power generation. Over-reliance on the ES will result in frequent charging, discharging, and a high ramp rate that can cause accelerated degradation. In literature, the impact of the operation load profile on the ES degradation is highlighted in [7,8] for the land-based power system. In [9], a general approach based on the forecast and the receding horizon is proposed for optimal operation while accounting for degradation reduction of the ES. Two-layer energy management of the microgrid with energy storage degradation cost is presented in [10]. However, these literatures mainly focus on the land-based power system and the optimal operation of the ES for the marine power system are yet to be explored. Furthermore, the operation of the ship power system is different from the land-based power system in the following ways, (1) fixed schedule for the grid-connected (at the harbor) and islanded mode of operation (during transit) (2) have higher ES to power system ratio (3) influenced by the propulsion requirements and port arrival time. These have to be accounted for in the modeling and design of the optimal scheduling of the ship.

As for the existing work in the literature for the optimal operation scheduling of ship power systems, a dynamic programming approach is used to limit greenhouse gas emissions with the help of ES in [21]. Rule-based and Grey wolf optimization methods are compared in [22] for fuel consumption minimization and emission reduction for the electric ferries. Interval optimization of the hybrid vessel with solar PV integration for the oil tanker is presented in [23]. It aims to minimize the fuel and emission cost while considering the investment cost of the ES. Generation and voyage scheduling with the demand-side response are presented in [14,17,24] which minimize fuel consumption by appropriately adjusting the propulsion speed of the vessel. The result proves that the optimal voyage scheduling will tend to benefit large vessels which have significant impact on the drag and hull

resistance coefficients with the adjustment in the propulsion speed. Despite the attempts to reduce the fuel consumption and emission, the operation scheduling of the ship power system is multi-objective in nature and the conflicting objectives of the system operation scheduling have to be carefully addressed. The vessel operators aim to optimize the operation cost (fuel consumption, cost of charging from the S2S power supply and maintenance cost), emission cost/carbon tax and ES degradation cost based on the operating scenarios. A single objective optimization approach will tend to result in over-reliance on the resources which are not considered in the objective function. In fact, there are not many studies on the optimal operation scheduling of ship power systems which consider all the aforementioned factors. Even if the multi-objective optimization methods are proposed, the performance analysis of the dispatch result of the multi-objective optimization is yet to be investigated. Furthermore, the effect of grid electricity price on the operation of hybrid vessels is not fully investigated. Thus, this paper investigates the optimal operation scheduling of the hybrid vessels that consider the grid electricity price of S2S power supply, renewable energy sources, ES degradation, and greenhouse gas emission with the help of multi-objective optimization.

To have a better understanding of the current state of the art for the ship power system operation scheduling, two recent studies with similar research direction with the proposed method in this study are identified. The selected research works on the optimal operation scheduling of the ship power system are illustrated in [25,26]. To highlight the key differences from the proposed approach in this study, comparison with the above references are illustrated. In [25], multi-objective operation scheduling of the ship power system is carried out with a meta-heuristic optimization approach by considering the operation cost and emission of the vessel. Similar work on the operation scheduling of a cruise vessel is also presented in [26] with very similar modeling and method as illustrated in [25]. It employs a multi-objective deterministic optimization to identify the optimal operating point of a cruise vessel. However, the aforementioned studies have yet to consider the potential integration of solar PV on-board the ship power system and how the solar irradiation variation will influence the final dispatch parameters of the multi-objective optimization of the vessel. For the proposed approach in this research work, the weight assignments of the multi-objective functions are carefully addressed by accounting the day-ahead prediction interval data of solar irradiation. A two-stage dispatch approach with different optimization time resolutions is also proposed to improve the dispatch accuracy and reliability of the vessel. The proposed approach also highlights and demonstrates that the selection of the optimal operating points for the hour-ahead operation from the Pareto solution front is not a trivial task from the vessel operator's point of view. Thus, detailed analysis such as the average rate of change of SOC and the Pareto front shifting with changes in the weight assignment and stochastic variable such as solar irradiation is required to be analyzed to provide a better understanding of the optimal operating point of the vessel. Such analyses are yet to be thoroughly explored and presented in the literature. Furthermore, the research works in [25,26] have yet to consider the impact of ES degradation in the multi-objective model. Generally, in the ship power system, ES is integrated not only to ensure the emission improvement but also to improve the generation dispatch reliability by acting as a spinning reserve, emergency energy reserve, or in the standby mode of operation. As a result of the high investment cost, the use of ES should be carefully designed and incorporated into the objective formulation. As the degradation of the ES is not considered in the above studies, the depth of discharge (DOD) of the ES is higher and hence significantly affects the life of the ES. The energy reserve of ES for the emergency mode of operation is also not adhered to in these studies. In this research work, the dispatch reliability is addressed by allowing the vessel operators to identify how the ES should be operated based on the solar PV generation. The energy reserve from the ES can be set by selecting an appropriate operating point from the Pareto front solution space. The weight assignment will also affect the ramp rate of the ES and hence vessel operators have more control over the way the vessel should be operated. Furthermore, these studies have yet to model the integration of S2S and how the grid electricity price will influence the energy exchange with the main grid. Moreover, the above study focuses on the multi-energy system which is only applicable to vessels with high thermal load demand

such as cruise ships. However, in this study, a more-electric vessel with a higher penetration of the ES and solar PV are addressed to cover the wider types of vessel in the marine industry. The detailed contributions of this research work are further summarized in the following section.

3. Contributions

The main contributions of this paper are summarized: (1) A two-stage multi-objective optimization problem is modeled for a hybrid vessel that encompasses the operation, emission, and ES degradation cost. The first stage (day-ahead) optimization attempts to map the solution space based on the PV interval prediction data for the performance comparison of the objective functions. From this, the optimal weights selection based on the user's preference is selected for the second stage (hour-ahead) with shorter-time and more accurate prediction data. It allows the vessel operators with a basic understanding of optimization to understand the differences in the dispatch strategy with the changes in the solar irradiation (2) Analytical model of the ES degradation is modeled to incorporate into the optimal scheduling of the ship power system. Static and dynamic degradation of ES are considered for optimal scheduling which are ignored in other literature. (3) The demand response electricity pricing of the S2S power supply is modeled to illustrate the accurate representation of the system which has grid charging or S2S capability. (4) The impact of the uncertainty nature of the PV on the weight assignment is addressed with two stages of optimization before and after the uncertainty realization. Case studies with a hybrid ferry are illustrated to demonstrate the proposed optimal scheduling. Hybrid ferry with shorter voyage distance and enough berthing duration is illustrated as a case study due to its potential benefit from the PV, ES, and S2S integration. However, there is a generality in the proposed approach and can be applied to any other type of vessel.

4. Proposed Optimal Dispatch Scheme of Hybrid Ferry with Shore-to-Ship Power Supply

The proposed optimal dispatch scheme of a hybrid ferry involves two stages of multi-objective optimizations. The main aim of the first stage of optimization is to map-out the Pareto front solution space based on the interval forecast data of the solar PV output and compare the performances of the different solution sets with the help of normalization. Mapping of the solution space is a time-consuming process and the optimal weights selection for the objective functions requires a detailed understanding of the performance of the model at different operating points in the solution space. Hence, the first stage of optimization is carried out prior to days ahead of the actual economic dispatch. As for the second stage of the economic dispatch scheme, weights selection of the objective functions is carried out based on the performance comparison on the normalized data set and the user's preference. With more accurate short lead-time point forecast data of the PV generation, the final dispatch is carried out for the hour-ahead dispatch. The detailed illustration of the proposed dispatch scheme is illustrated in Figure 1.

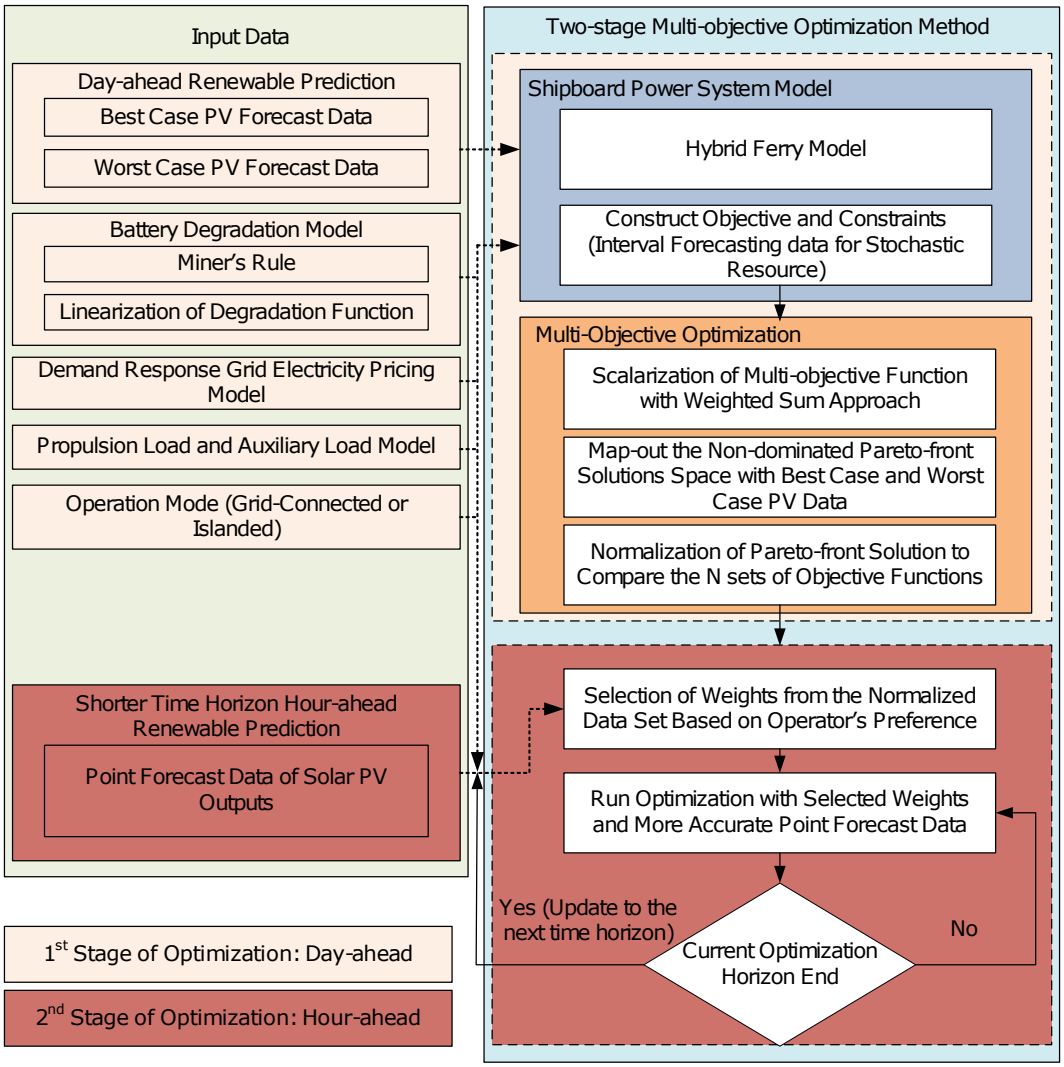

Figure 1. Proposed framework for multi-objective optimization in hybrid ferry.

5. Mathematical Modeling

In this section, mathematical modeling of ship power system is illustrated. Generation, storage, and operation constraints and objectives are illustrated in the following subsections.

5.1. Energy Storage Degradation Model

Although it is important to measure the state of health (SOH) of the ES for safe and reliable operation, it is still a very challenging and complex task due to the complex interaction of the chemistry in ES system. Thus, ES manufacturers generally provide the number of cycles promised and depth of discharge (DOD) as the key measures to estimate the SOH of the ES. The number of half-cycles with respect to the DOD provided by the manufacturer [27] is shown in Figure 2. Exponential curve fitting is carried out to derive the fitting coefficient to defines the relationship between cycle life and DOD in (1). To reduce the computational effort of non-linear function, Equation (1) is linearized into two piece-wise linear functions as shown in (2). For the two piece-wise linear functions, the goodness of fits are provided as R-square values based on the data points given in [27]. The fitting range or the interval of the linear functions are also determined based on the R-square values of the fitting. For the piece-wise approximation from 20% to 40%, R-square value is 0.9658. Similarly, the piece-wise approximation between 40% to 60%, the R-square value is 0.9782. Larger number of piece-wise functions can also be used to represent the relationship between the number of half-cycles and depth of discharge to further

improve the accuracy of the approximation without compromising the efficiency of the computational time. This is because the search space for the optimal solution remain unchanged with the increase in number of piece-wise representation. However, the R-square values indicate that the two piece-wise linear fittings are sufficiently represented and fit to be used for the degradation model of the ES.

$$N_{DOD} = \alpha_0 \times e^{(\alpha_1 \times DOD)} \tag{1}$$

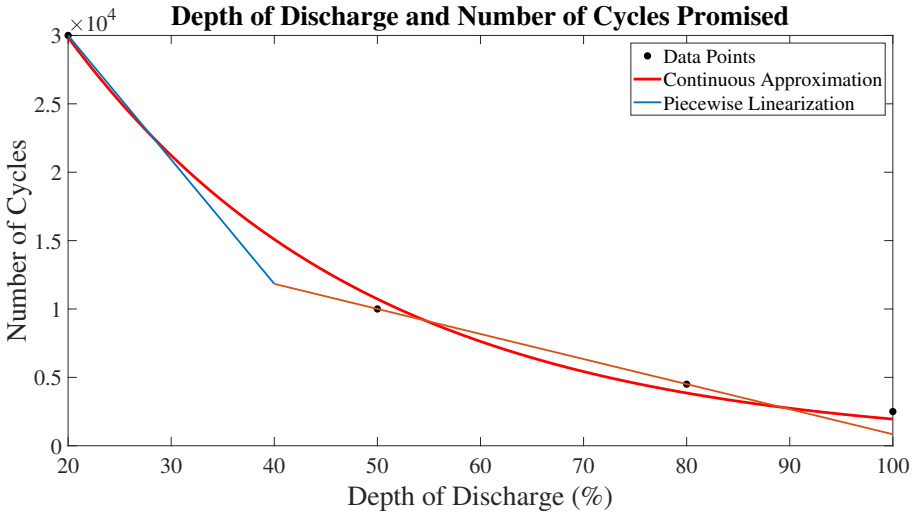

Figure 2. Relationship between number of cycles with depth of discharge.

ES degradation can occur during storage and usage. These are termed as static and dynamic degradation. Common failure mechanisms of the static degradation are corrosion of electrodes and the oxidation of electrolyte whereas dynamic degradation is mostly influenced by the thermal and electrical stresses due to cycling, operating environment, and DOD. Although impedance measurement is a good estimate of the ES degradation and remaining useful life, it is a complicated and time-consuming procedure for real-life application. Thus, as an alternative, cycle life depreciation is used to estimate the health of the ES in most applications.

$$N_{DOD} = \begin{cases} a_1 \times DOD + b_1, 20\% \leq DOD \leq 40\% \\ a_2 \times DOD + b_2, 40\% < DOD \leq 80\% \end{cases} \tag{2}$$

The ES cycle life is the number of complete charge and discharge cycles that the ES can support before its end of life. The analytical degradation model proposed in this study makes the following assumptions. The degradation due to the changes in temperature is carefully minimized with a cooling system, the relationship between cycle life and the DOD are accurately modeled by the manufacturers and the effects are independent of the battery age for a short duration simulation. After a long period of usage, the relationship between the DOD and the number of half-cycles will have to be updated by adjusting the curve fitting coefficient based on the capacity retention factors and other test data from the ES manufacturer [7–9]. These assumptions allow the model to be simple enough for a quick evaluation and accurate enough for the analysis of the degradation. With these assumptions, Miner's rule [28] is employed to account for the number of cycles that are being depreciated or used from ES. By associating the cycle life and DOD, Miner's rule is used to construct approximate equations for static and dynamic degradation of the ES.

With the aforementioned assumption, the static degradation of the ES is assumed as linear throughout its shelf life and can be expressed as shown in (3). The dynamic degradation of the ES is modeled based on the variation of the SOC of the ES in small regular time-step over the study period. Hence, the non-linear nature of the ES can be approximated accurately. Degradation from the incomplete charge and discharge cycles can be approximated with (4). To accurately represent the dynamic

degradation, it will be calculated at every sampling instance of the optimization. The accumulated cycle used over the study period is illustrated in (5) and (6). However, solving non-linear equations in (4) is computationally intensive. To reduce the computational effort, linear degradation of ES is used with a slight modification of the model in (4). With the approximate linear representation between cycle life and DOD as shown in (2), dynamic degradation per half-cycle from DOD of i% to j% is linearized as shown in (7).

$$\gamma_s = \frac{1}{2 \times N_{static} \times t_{lt,ES}} \times T \tag{3}$$

$$\gamma_d = \sum_{t=2}^{T} \left| \frac{1}{2 \times N_{DOD}(t)} - \frac{1}{2 \times N_{DOD}(t-1)} \right| \tag{4}$$

$$\gamma_{acc} = \gamma_s + \gamma_d \tag{5}$$

$$\sum_{t=1}^{t_{lt,ES}} \gamma_{acc}(t) = 1 \tag{6}$$

$$\gamma_d = \frac{1}{2} \left| \frac{1}{N_{DOD,i\%}} - \frac{1}{N_{DOD,j\%}} \right|, i\% \leq DOD \leq j\% \tag{7}$$

5.2. Propulsion Load Model

The propulsion load is approximated from a given speed profile. It depends on the resistance of the hull and the operating condition of the vessel. It can be approximated with (8) [14,17]. The typical load profile of a ferry is generally categorized into 5 different operation modes; departing harbor, acceleration, approaching harbor, cruising, and at the harbor. Since ferries tend to follow a regular travel route, operating speed, and have smaller form factor to have significant effects with propulsion adjustment, voyage scheduling is not carried out in this study.

$$P_{\mathrm{Pr}op} = c_{P1} \times v^{c_{P2}} \tag{8}$$

5.3. Demand Response Electricity Price Model

S2S is an appropriate solution to make harbors free from greenhouse gas emission and air pollutants while the vessel is at berth. In this study, it is assumed that the shore area is sufficiently designed and well-equipped for the S2S power supply and they are directly supplied by the electricity providers from the main grid. Thus, demand response electricity pricing is modeled for S2S and is illustrated in (9). The grid electricity price is dependent on the amount of electricity acquired from the ship power system. The scaling factor ζ is introduced to account for the inflation factor for the service provision from the grid. It can be due to the infrastructure improvement or the grid congestion at the time of demand. The proposed demand response pricing model is inspired by the demand response pricing schemes that are implemented in the industry [29].

$$F_{ele}(t) = f_{TOU}(t) \times \left(1 + \zeta \times \frac{P_{grid}(t)}{P_{grid,\max}} \right) \tag{9}$$

5.4. Hybrid Vessel Operation Model

In this study, the objectives of the optimal scheduling of ferries are to reduce the operation cost of the ferry such as fuel consumption, maintenance, emission, and grid charging while reducing the ES degradation. The objectives are categorized to form two conflicting functions that are related by the weighted coefficients; w_1 and w_2 as shown in (10). The detailed representations of the objectives are illustrated in (11)–(17). For clarity, associative objectives which are weighted with the coefficient w_1 and w_2 will be termed as objective 1 and objective 2 for the remaining of the paper. It is worthwhile

to note that individual weights can be assigned to objective terms from (11)–(17). Nonetheless, it is more computationally intensive with the increase in number of separate objectives. Hence, based on the prior literature survey and initial simulation results, the cooperative objectives and conflicting objectives are identified [13,14,17–19].

$$\min w_1(\text{cost}_{fuel} + \text{cost}_{SC/SD} + \text{cost}_{mai}^{DG} + \text{cost}_{mai}^{PV} + \text{cost}_{grid} + \text{cost}_{emission}) + w_2\text{cost}_{ESS,\text{deg}} \tag{10}$$

$$\text{cost}_{fuel} = \sum_{t=1}^{T}\sum_{n=1}^{N} F_{fuel} \times \Delta t \times FC_{DG}^{n}(t) \tag{11}$$

$$\text{cost}_{SC/SD} = \sum_{t=1}^{T}\sum_{n=1}^{N} |u_{DG}^{n}(t) - u_{DG}^{n}(t+1)| \times F_{trans} \tag{12}$$

$$\text{cost}_{mai}^{DG} = \sum_{t=1}^{T}\sum_{n=1}^{N} F_{DG,mai} \times P_{DG}^{n}(t) \times \Delta t \tag{13}$$

$$\text{cost}_{mai}^{PV} = \sum_{t=1}^{T} F_{PV,mai} \times P_{PV}(t) \times \Delta t \tag{14}$$

$$\text{cost}_{grid} = \sum_{t=1}^{T} P_{grid}(t) \times F_{ele}(t) \times \Delta t \tag{15}$$

$$\text{cost}_{emission} = \sum_{t=1}^{T}\sum_{n=1}^{N} F_{co2} \times c_{co2} \times FC_{DG}^{n}(t) \times \Delta t \tag{16}$$

$$\text{cost}_{ESS,\text{deg}} = \text{Total Life Cycle Cost} \times \sum_{t=1}^{T} \gamma_{acc} \tag{17}$$

$$\text{Total Life Cycle Cost} = I_{ESS} - \frac{Sl_{ESS}}{(1+r)^{T}} + \sum_{t=1}^{T} \frac{OM_{ESS}}{(1+r)^{t}} + \sum_{t=1}^{T} \frac{F_{ch,ave} \times N_{ave} \times E_{ESS,rated}}{(1+r)^{t}} \tag{18}$$

$$I_{ESS} = S_{ESS,rated} \times E_{ESS,rated} \tag{19}$$

DGs' fuel consumption is computed with (11). Smaller DGs on ferries tend to have lower state transition costs. However, to lower the number of state transitions, the total cost of state transition as shown in (12) is used. The total DGs and PV maintenance cost are illustrated in (13) and (14). The total cost of S2S operation is expressed in (15). The total carbon tax due to emission is calculated as shown in (16). As shown in (17), total ES degradation cost is modeled as the amount of life cycle cost that is being depreciated from its usage. The total life cycle cost of the ES in (18) is a function of the initial investment cost, salvage cost, operation and maintenance cost, and charging cost. The initial investment cost as shown in (19) is a one-time cost incurred at the start of the project. In contrast, the operation and maintenance cost (OM) are incurred throughout the operational lifecycle. ES is required to be charged for it to be used and the cost of charging is accounted for when calculating the life cycle cost of the ES. Aggregated average charging price of electricity is used as the future value of the grid electricity price. The scaling factor $1/(1+r)^t$ is the conversion factor of the future value to the present value in the total life cycle cost calculation.

$$\sum_{i=1}^{N} P_{DG}^{n}(t) + P_{grid}(t) + P_{dis}(t) + P_{PV}(t) = P_{load}(t) + P_{ch}(t) \tag{20}$$

$$P_{DG,\min}^{n} \le P_{DG}^{n}(t) \le P_{DG,\max}^{n} \tag{21}$$

$$\frac{\left|P_{DG}^{n}(t) - P_{DG}^{n}(t-1)\right|}{\Delta t} \le P_{\text{ramp,max}}^{n} \tag{22}$$

$$\left|u_{DG}^{n}(t_{on/off}) - u_{DG}^{n}(t_{off/on})\right| \geq t_{DG}^{n,\min on/off} \tag{23}$$

$$P_{grid,\min} \leq P_{grid}(t) \leq P_{grid,\max} \tag{24}$$

$$SOC_{\min} \leq SOC(t) \leq SOC_{\max} \tag{25}$$

$$SOC(t) = SOC(t-1) + \frac{[\eta_{ch} \times P_{ch}(t) \times \Delta t] - \left[\frac{P_{dis}(t)}{\eta_{dis}} \times \Delta t\right]}{E_{ESS,rated}} \times 100 \tag{26}$$

$$P_{ch,\min} \times u_{ESS}^{'}(t) \leq P_{ch}(t) \leq P_{ch,\max} \times u_{ESS}^{'}(t) \tag{27}$$

$$P_{dis,\min} \times u_{ESS}(t) \leq P_{dis}(t) \leq P_{dis,\max} \times u_{ESS}(t) \tag{28}$$

$$FC_{DG}^{n} = a_n \times (P_{DG}^{n})^2 + b_n \times P_{DG}^{n} + c_n \tag{29}$$

$$[P_{PV,\min}(t), P_{PV,\max}(t)] = \eta_{PV}(t) \times A_{PV} \times \left[Irr_{PV,\min}(t), Irr_{PV,\max}(t)\right] \tag{30}$$

Mathematical model of the ship power system is employed and the detailed operating constraint of the ship power system is illustrated in this section [13,14,17–19,21–24]. The power balance constraint in the ferry is shown in (20). In (21)–(23), the loading factor, ramp rate and minimum up/down time constraints of the DGs are specified. Minimum and maximum power exchange with the S2S power supply are shown in (24). ES SOC limits are specified in (25) and updated with (26). The ES maximum and minimum charge/discharge power limits are illustrated in (27) and (28). The DGs fuel consumption which is a factor of loading factor is approximated as shown in (29). PV output based on irradiation is carried out as interval forecast data in this study and illustrated in (30).

6. Solution Methods

The compact form of the solution methods, programming language and solver used are further illustrated in this section. The optimization problem is scalarized linearly with the weighted sum approach in this study. The scalarization of the objective functions in (10) is governed by (31). Due to non-dominated solutions, the key challenge with the multi-objective problem is to select the operation point. Hence, in this study, the mapping of the solution space based on the day-ahead PV prediction data is carried out to allow the vessel operators to comprehend the operating points prior to the actual optimal dispatch (hour-ahead). The proposed optimal dispatch problem and solution method are model in MATLAB with YALMIP and solve using CPLEX solver [30,31]. Once the Pareto front solution sets are identified with the iteration process, the multi-objective decision-making process must be carried out to select the optimal trade-off between the objectives. One of the challenges with trade-off analysis in the multi-objective optimization is that the comparison vectors are non-commensurable due to the large difference in the numerical value. This can be overcome with the normalization of the solution vectors ($N = [N_{11}, N_{12}, \ldots, N_{nm}]$) over the positive range between 0 and 1 without changing their physical meaning or representation. Hence, in this study, normalization is carried out to compare the Pareto solution sets. Assuming there are n-dimensional Pareto solution sets for m-dimension objectives, the normalization of the individual objective criteria can be carried out for each Pareto solution set as shown in (32) [26]. Once the normalization is carried out, the optimal operating point can be identified by calculating the Euclidean distance from the user preference operation point.

$$F(x) = \sum_{i=1}^{m} w_i \times f_i(x), w_i \geq 0, \sum_{i=1}^{m} w_i = 1 \tag{31}$$

$$N_{i,j} = \frac{(f_{i,j} - f_{j,\min})}{(f_{j,\max} - f_{j,\min})}; \begin{cases} i = 1, \ldots, n \\ j = 1, \ldots, m \end{cases} \tag{32}$$

7. Case Study Parameters

This section will elaborate the vessel under study and its operating parameters to be used for the case study.

7.1. System Configuration and Parameters

Power system architecture of the ferry is illustrated in Figure 3. It is 80 m in length and 21.5 m in breadth, and 70% of the space is installed with PV. Interval prediction of the solar irradiation data is obtained from the Energy Market Authority in Singapore [29] and illustrated in Figure 4. The parameters for the constraint formulation are provided in Tables 1 and 2. The fuel consumption curve fitting coefficients (a, b, c) of the DG1 and DG2 are also illustrated in Table 1. It is worthwhile to mention that the investment of the ES are assumed to be relatively large and this is due to the fact that it has accounted for the energy conversion devices on board the ship. Similarly, the maintenance costs of the PV are higher due to the corrosion effect of the salty water and hence it has to be well maintained as compared to the land-based system.

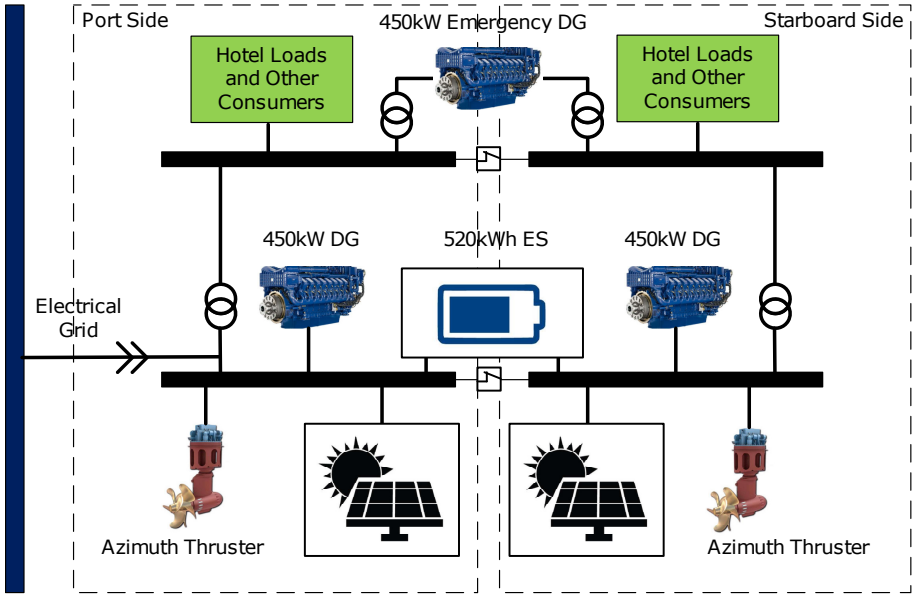

Figure 3. Single line diagram of hybrid-electric ferry with grid integration.

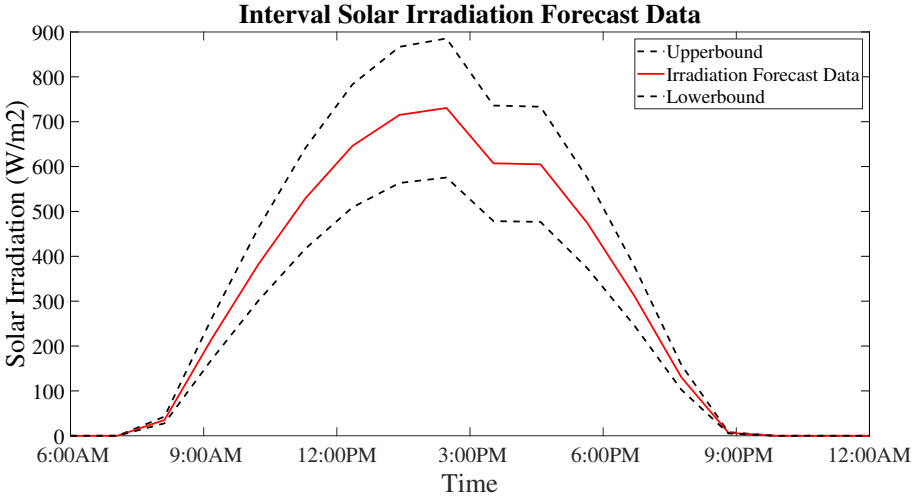

Figure 4. Interval solar irradiation forecast data in Singapore—5 February 2019.

Table 1. Operation and economic parameters for diesel generator, grid, and photovoltaic (PV) [32,33].

Unit	$P_{\max}$ (kW)	$P_{\min}$ (kW)	$T_{\min}$ (min)	$P_{ramp,\max}$
DG1	450	200	15	200 (kW/Δt)
DG2	450	200	15	200 (kW/Δt)
Grid	300	0	–	–
DG1	$a = 1.568 \times 10^{-4}$, $b = 0.592$, $c = 0.0001$			
DG2	$a = 6.72 \times 10^{-5}$, $b = 0.160$, $c = -0.0001$			
F_{fuel} = 0.83 \$/L, F_{CO_2} = 30 \$/ton, F_{trans} = 10 \$/transition				
$F_{DG,mai}$ = 0.007 \$/kWh, $F_{PV,mai}$ = 0.05 \$/kWh, Δt = 5 min				

Table 2. Operation and economic parameters for hybrid energy storage systems [34].

$P_{ch/dis,\max}$ 300 kW	$P_{ch/dis,\min}$ 0 kW	η 97%	$SOC_{\min}$ 40%	$SOC_{\max}$ 80%
$E_{ESS,rated}$ 520 kWh	γ_s 10/year	α_1 −0.03411	α_0 59,070	a_1 −908
b_1 4.816×10^4	a_2 −183.3	b_2 1.917×10^4	T 10	$S_{ESS,rated}$ 1500 \$/kWh
N_{ave} 1000	$F_{ch,ave}$ \$78,000	r 0.12 \$/kWh	Sl_{ESS} 5%	OM_{ESS} 14.55 \$/kW

7.2. Vessel Operating Profile

The speed profile inspired by the Ampere ferry [6] is used for the longer voyage between Singapore and Batam Island which is about 34 km away. The speed profile is illustrated in Figure 5 and the transit takes about an hour with the average traveling speed of 13–15 knots. The vessel remains at the harbor for 30 min for charging of the ES, embarking, and disembarking. The loads are categorized into propulsion and hotel load. For simplicity, hotel loads are assumed to be constant at two different levels; 200 kW during the sail and 250 kW when the ferry is at the harbor. Propulsion load requirements are derived from (8); 675 kW during departing, 720 kW during acceleration, 500 kW during cruising, 520 kW while approaching harbor, and 50 kW at the harbor for station-keeping, embarking and disembarking. The estimated total power demand of the vessel is illustrated in Figure 5.

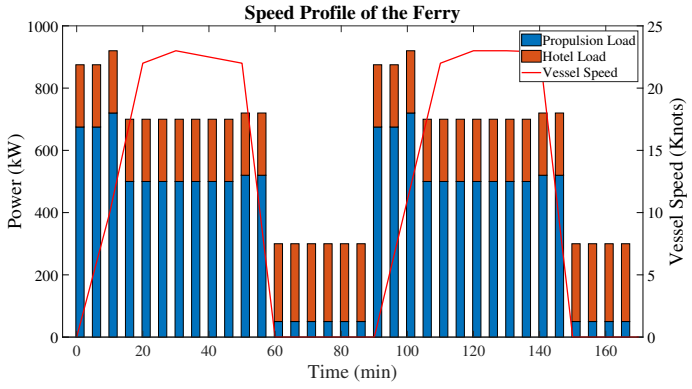

Figure 5. Typical Speed and Load Profile of the Ferry.

8. Simulation Results

The simulation results are split into two subsections. The first subsection will elaborate the results obtained from day-ahead scheduling or solution space mapping based on solar interval PV prediction data whereas the second subsection will elaborate in details of the hour-ahead generation dispatch.

The simulations were carried out on on an Intel(R) Xeon(R) E5-1630 3.70 GHz 64-bit PC with 16 G RAM and solved by the commercial CPLEX solver.

8.1. First Stage of Optimal Dispatch—Day-Ahead

In the first stage, various sets of weight governed by (31) were assigned to the two objectives in (10) to establish the solution space. Table 3 lists the cost values of the objective functions with a various sets of weights. The simulation times are also provided in the same table. As a comparison, the non-linear optimization with the degradation model in (4) with branch and bound method took more than 3 h to complete for a single set of weight. The simulation time depends on the optimization time-resolution, optimization horizon, number of decision variables, and the operating range of the constraints. By comparing the simulation time, it was concluded that the linearization of the ES degradation function can significantly improve the simulation time. It is also worthwhile to mention that day-ahead operation scheduling of the ship power system were generally carried out just a day ahead before the actual operation. This was because the ship power system needed to estimate the propulsion power requirement of the vessel based on the sea-state and payload with the help of the Equation (8). Forecast data of the solar irradiation was also required to be carried out in the proposed model. For the solar irradiation forecasting, the longer lead-time from the actual operation resulted in higher uncertainty in the prediction and hence making the Pareto front solution space with the longer lead-time to become insignificant or redundant. From Table 3, it is observed that the largest change in the objectives occurred between $w_1 = 0.8$, $w_2 = 0.2$ and $w_1 = 0.6$, $w_2 = 0.4$. It is the point of interest in the solution space, as there was high fidelity on the trade off between the objectives. From the simulation time as shown in Table 3, it also reflected the conflicting nature of the objective functions at these sets of weight as the computation time of the optimization significantly increased. The set of weights $w_1 = 1$, $w_2 = 0$ and $w_1 = 0$, $w_2 = 1$ represent the optimization of the single objective function and the cost values obtained from these optimizations are the optimal point of operation to reduced the specific objective in the multi-objective optimization. For an example, if w_1 was assigned a value of 1, the minimum cost of emission, fuel consumption, and operation cost and the maximum value of ES degradation were obtained from the above optimization. These sets of weights could be used as benchmarks to evaluate the performance of the remaining solution. From Table 3, if only objective 1 was optimized, the cost of operation, fuel consumption and emission improved up to 46.93%. This is proven in many literature that are discussed in detailed in the literature review section. On the other hand, the single objective optimization of objective function 2 improved the ES degradation up to 99.95%. However, in reality, the set points $w_1 = 0$, $w_2 = 1$ were almost equivalent to the system operation with no ES and hence the cost of operation could be drastically reduced for the objective function 2. Given these extrema of the objective functions, it becomes clear that there should be a systematic way to analyse the solution space of the Pareto front and identified an optimal operating point of the ship power system to achieve the overall objective of the conflicting objectives in the model.

Figure 6 illustrates the solution space of the optimization. More data points between $w_1 = 0.8$, $w_2 = 0.2$ and $w_1 = 0.6$, $w_2 = 0.4$ are included to map out the solution space. With the assumption that the solar interval prediction was accurate and had similar output characteristics and shapes for the following day, any possible solutions were bounded by this solution space. Figure 7 illustrates the normalized effect of the solution space against weight w_1. Users could observe the performance of objective 1 and 2, and decide the sets of weight to be used with (10) in the second stage of dispatch. From the result, the weight w_1 between 0.61 to 0.65 resulted in the effects of the objective 1 and 2 having a similar response from each other whereas the weights above these values gave more emphasis on the objective 1 and values below these provided more emphasis on objective 2. The area bounded by the dashed line and solid line in Figure 7 was the confident bounds due to the interval forecast data of the solar irradiation. It also illustrated the influence of the penetration of the solar PV on the objective functions. The average change in the SOC and energy with the changes in the weight assignments is illustrated in Figure 8. With greater emphasis to reduce the degradation, the ES was not utilized

effectively. If it was not considered in the objective formulation, the degradation cost was even close to the cost of emission and fuel consumption, indicating the over reliance of the ESS. It should be highlighted again that the degradation cost of the ES was large because it considered degradation, charging, and power conversion cost in the total life cycle cost formulation. Furthermore, Figure 8 also highlights that with the increase in emphasis of w_1, the rate of change of energy for the ES increased up to 16 kWh/5 min which was equivalent to a ramp rate of 192 kW for the optimization. Although charging and discharging of ES are rated higher than the above ramp rate limits in the simulation, such transient behavior of the charging and discharging characteristic of the ES will significantly affect the life of the ES and hence should be carefully addressed.

Table 3. Cost distribution of objective functions for solar irradiation interval.

Weight (w)	PV Bound	Objective 1-Emission, Fuel Consumption and O&M Cost $	Objective 2-Energy Storage Degradation Cost $	Simulation Time (s)
$w_1 = 1.0$	Upper	1.99×10^3	1.80×10^3	0.80
$w_2 = 0$	Lower	2.14×10^3	1.80×10^3	0.87
$w_1 = 0.9$	Upper	1.98×10^3	1.79×10^3	1.93
$w_2 = 0.1$	Lower	2.14×10^3	1.80×10^3	1.83
$w_1 = 0.8$	Upper	2.00×10^3	1.66×10^3	3.48
$w_2 = 0.2$	Lower	2.14×10^3	1.80×10^3	3.45
$w_1 = 0.7$	Upper	2.12×10^3	1.32×10^3	5.36
$w_2 = 0.3$	Lower	2.28×10^3	1.40×10^3	5.38
$w_1 = 0.6$	Upper	2.53×10^3	488.78	9.61
$w_2 = 0.4$	Lower	2.90×10^3	170.00	9.60
$w_1 = 0.5$	Upper	2.76×10^3	193.18	14.94
$w_2 = 0.5$	Lower	2.96×10^3	105.15	15.21
$w_1 = 0.4$	Upper	2.87×10^3	123.60	10.81
$w_2 = 0.6$	Lower	2.96×10^3	105.15	11.21
$w_1 = 0.3$	Upper	2.92×10^3	93.21	5.27
$w_2 = 0.7$	Lower	2.98×10^3	95.47	5.39
$w_1 = 0.2$	Upper	2.95×10^3	85.19	2.95
$w_2 = 0.8$	Lower	3.00×10^3	87.27	3.21
$w_1 = 0.1$	Upper	2.95×10^3	85.19	1.59
$w_2 = 0.9$	Lower	3.02×10^3	85.22	1.68
$w_1 = 0$	Upper	3.54×10^3	84.58	0.78
$w_2 = 1.0$	Lower	3.75×10^3	84.49	0.81

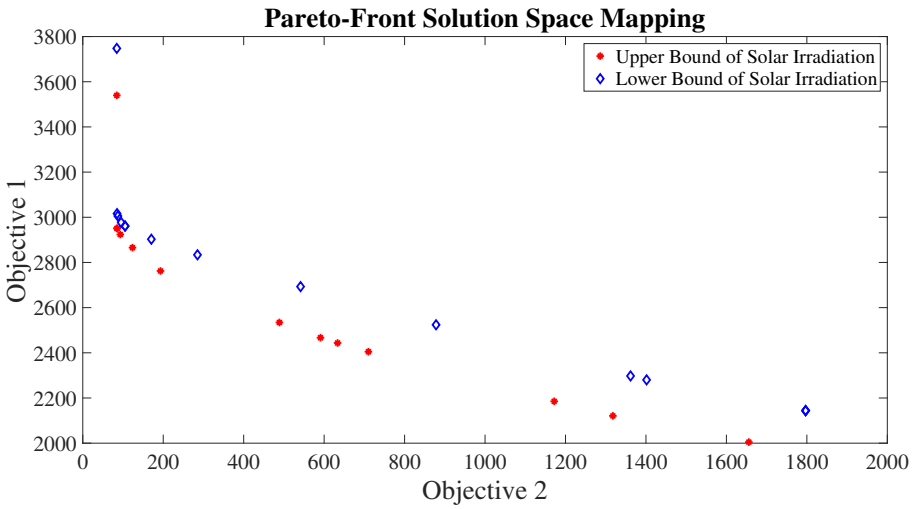

Figure 6. Pareto-front solution space with the interval solar irradiation forecast.

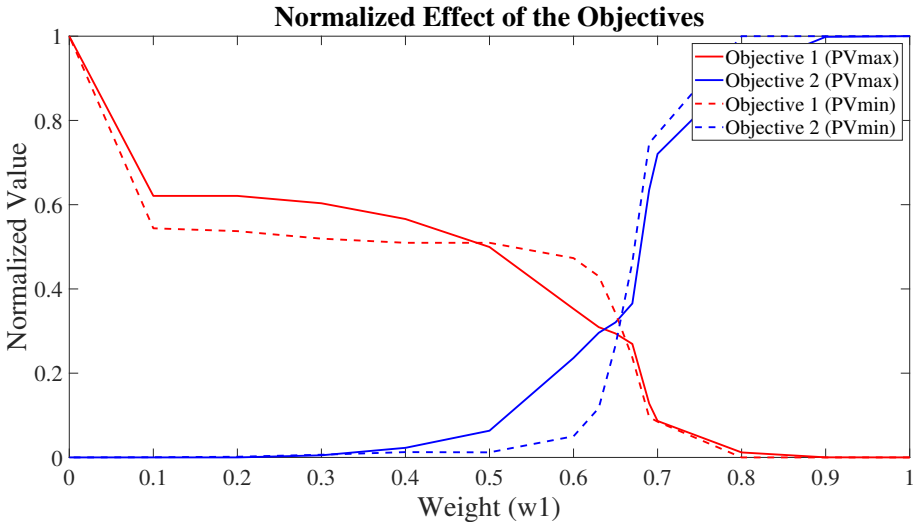

Figure 7. Normalized effect of the multi-objectives function.

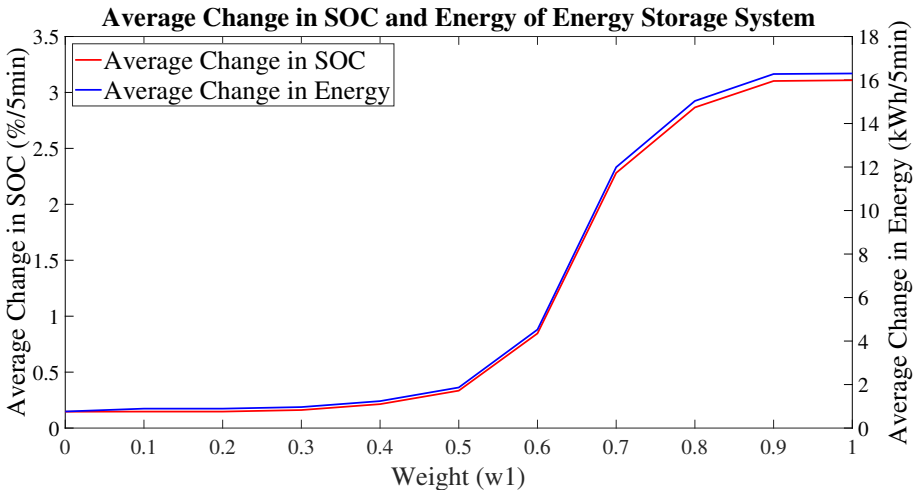

Figure 8. Average change in SOC and energy per unit time step of the energy storage system with varying weight w_1.

8.2. Second Stage of Economic Dispatch—Hour-Ahead

In the second stage, a more accurate point forecast data was used for the optimization process. In this study, it was assumed that the point forecast data lay within the prediction interval and followed a similar characteristic that is employed in the first stage of optimization. Hence, it did not result in any significant changes to the response, confident bounds and weights distribution identified in the earlier section. Mid-point average data that was used in the second stage of optimization is provided in Figure 9. To illustrate the differences in the dispatching scheme with the changes in the weight assignment, two case studies are illustrated. The dispatch results for the second stage of optimization forin Figures 10–15. In the case study 1, the emphasis on the two objectives was balanced out whereas the case study 2 emphasized more on the improvement in the objective function 1 for further comparison.

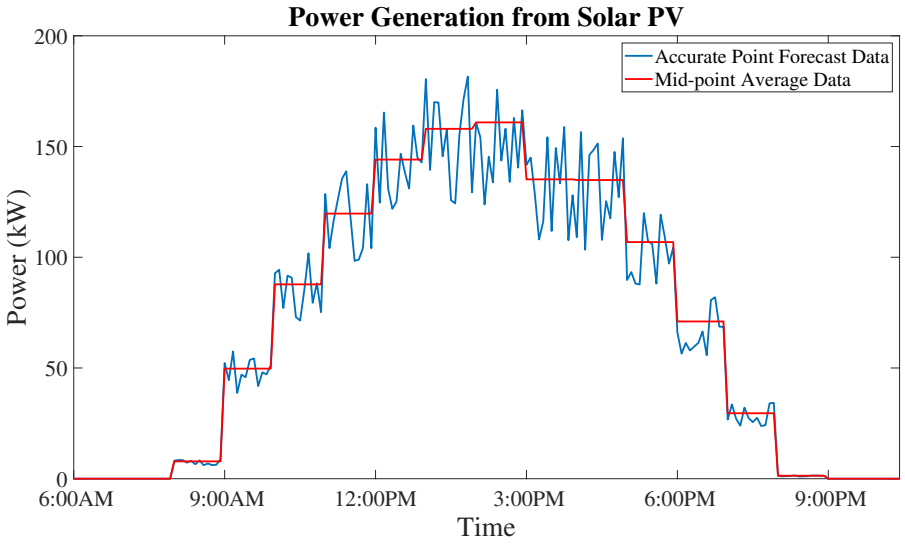

Figure 9. Mid-point average photovoltaic power generation.

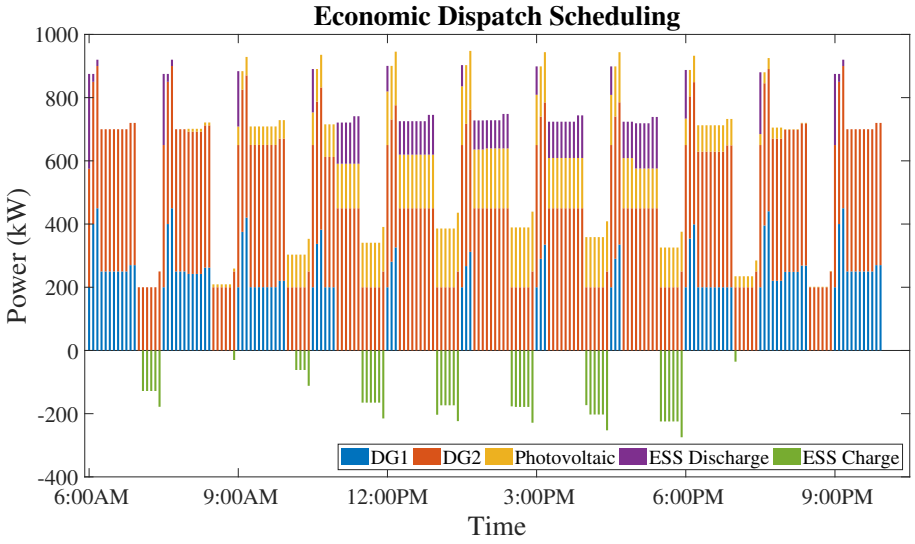

Figure 10. Economic dispatch for ferry generation scheduling (case study 1).

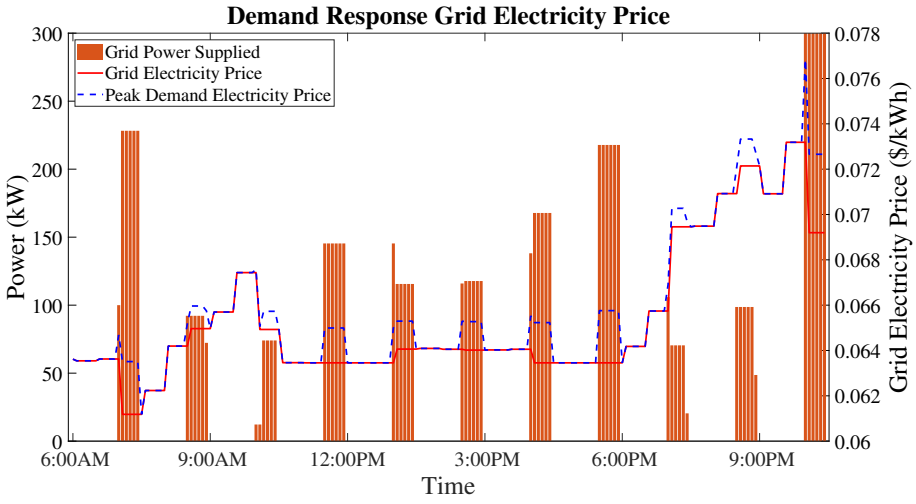

Figure 11. Shore-to-ship (S2S) power demand and peak demand response electricity price (case study 1).

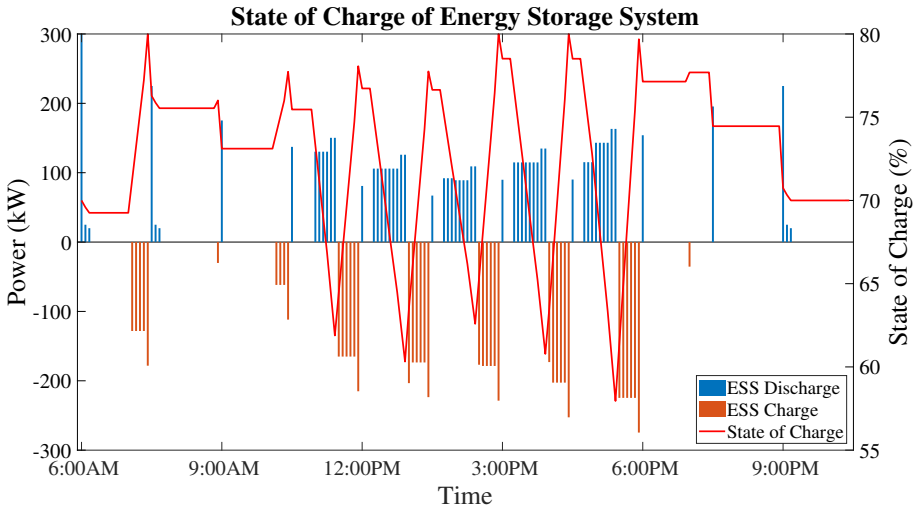

Figure 12. State of charge of energy storage system (case study 1).

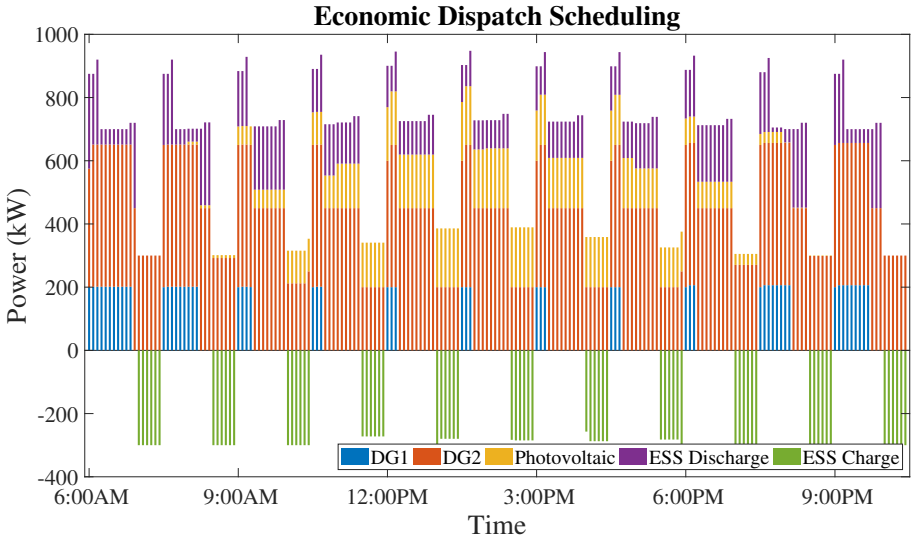

Figure 13. Economic dispatch for ferry generation scheduling (case study 2).

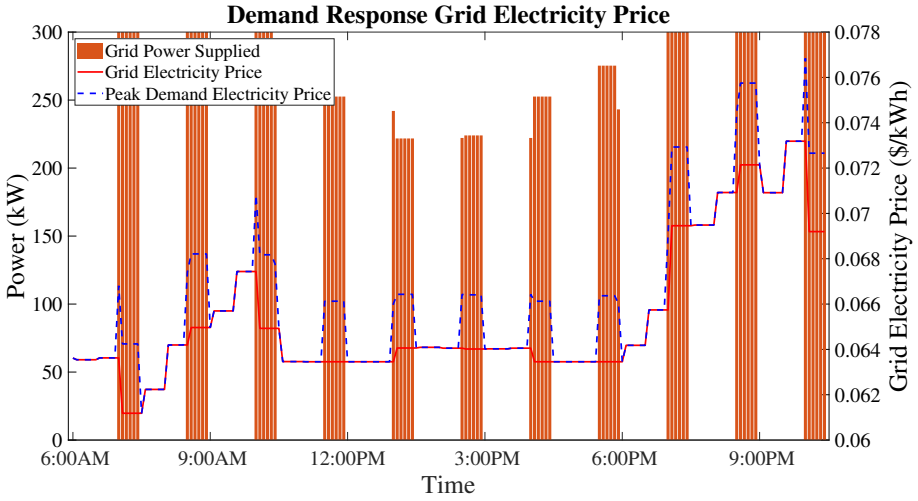

Figure 14. S2S power demand and peak demand response electricity price (case study 2).

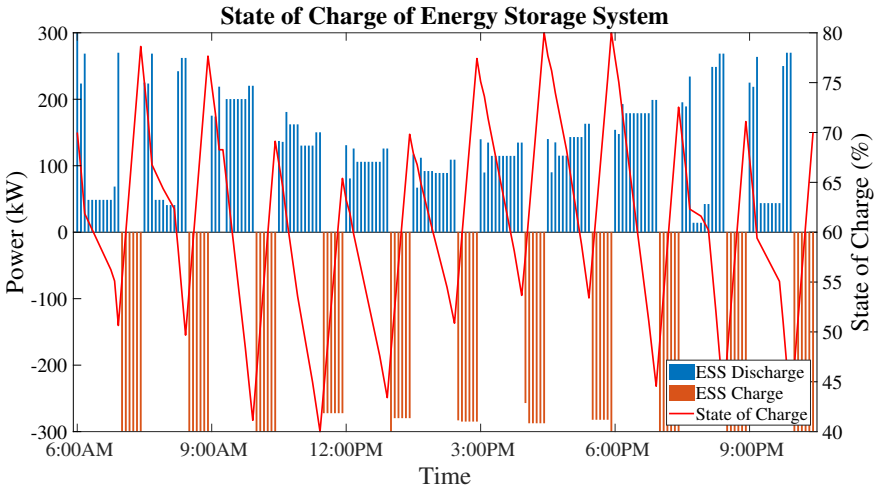

Figure 15. State of charge of energy storage system (case study 2).

8.2.1. Case Study 1—w_1 = 0.65 and w_2 = 0.35

For the remaining section of the case study, the weight assignment of the objective function 1 (w_1) and 2 (w_2) were treated as 0.65 and 0.35. This operating point was selected based on the normalized effect of the multi-objective function illustrated in Figure 7. It was the point where the similar improvements of the objective function 1 and 2 were achieved with regard to their respective objective maxima value. When a similar emphasis was specified to improve both objectives, ES was mainly used during the acceleration for departure and the constant speed cruising of the ferry as shown in Figure 10. The costlier generator DG1 was only employed when there was a significant power deficit from solar power generation or when the load demands were much higher. It can be observed that DG1 was mainly used in time instances such as 6:00 AM to 10:00 AM and 6:00 PM to the end of the operation for the lack of solar PV generation. Aside from these duration, DG1 was employed only for the acceleration mode of operation. Furthermore, DG2 was always loaded to its optimal loading condition (around 440 kW) before the start of the DG1 to ensure fuel and emission optimality. It can also be observed that ES was mostly used during mid-day to supplement power output from the solar power generation to prevent the prolonged use of the DG1 or starting of the DG1. ES was mainly charged from the S2S power supply during the berthing duration. This is because the grid electricity price to charge the ESS was relatively lower than the power generated from the DGs. Nonetheless, the amount of charging and discharging of the ES was limited due to the strong emphasis on minimizing the ES degradation. It is also worthwhile to point out that the optimization resolution was set to 5 min intervals to have a higher dispatch accuracy.

In Figure 11, the power demand profile for the S2S is illustrated. Most of the power demand from the grid was used to meet the load requirement during berthing and station keeping of the ferry as well as to charge the ES. The power demand from the grid was maximum at most time instances except for the mid-day where there was additional support from the solar PV. The demand response grid electricity price increased with the increase in the load demand from the S2S power supply and it is illustrated in Figure 11. When grid electricity price was lower or when the scaling factor (ζ) for the inflation of electricity price was lower, charging and discharging of the ES was more favorable. By comparing with Figure 12, the ES was charged from the grid at 7:30 AM to 8:00 AM as well as 12:00 PM to 6:00 PM as the grid electricity price were relatively lower as compared to other time instances. The optimization algorithm tried to balance the power demand from the grid and the DGs while at the harbor to ensure the economic benefit, fuel consumption, and emission minimization. It is worthwhile to note the S2S power supply was insufficient for the load demand of the vessel when the vessel was at harbor. Hence, DG2 was forced to be committed to its minimum loading capacity when the vessel was at harbor. However, if larger rating of the S2S was used in the simulation, all the DGs were turned off during the harbor. This is because the cost of the grid electricity price erre relatively cheaper than the DGs and the emission resulting from the low loading condition of the DGs was unfavourable. It can

also be observed that the demand from the grid was lowered when there was significant support from the solar PV generation. From Figure 12, it can be observed that the ES was mainly used during mid-day. As elaborated earlier, it was used as a supplement to the power output from the solar power generation to prevent the starting of DG1. It is also worth noting that the SOC of the ES was maintained above 55% and hence the DOD of the ES was within the healthier range of operation. Furthermore, 55% of the energy from the ES was ensured as the energy reserve for the emergency operation conditions. Hence, it can be concluded from the detailed simulation results that the dispatch results were highly influenced by many factors and the proposed scheme allowed the ship operators to have more flexibility in their optimal dispatch while providing a better understanding of the trade-off in the objectives of the chosen dispatch scheme. For the above weight distribution, the cost distributions of objective functions 1 and 2 were 2.54×10^3 and 632.27. It also means that the improvements of the objective functions 1 and 2 were 28.25% and 64.9% improvement from their respective maxima values. By comparing with the single objective optimization results illustrated in Section 8.1, it was proven that the optimal trade off between the two objective functions was achieved based on the weights distribution of the objective functions and updated solar PV irradiation data. Hence, the results obtained are satisfactory for the overall vessel operation.

8.2.2. Case Study 2—$w_1 = 0.85$ and $w_2 = 0.15$

To compare and appreciate the results obtained from the case study 1, case study 2 which is generally aligned with what is currently done in the literature is presented. Case study 2 emphasized more on the optimization of operation cost, fuel consumption, and emission tax. When more emphasis was being paid to the objective function 1, it was observed that the economic dispatch utilized the ES more frequently. In most of the operation scenarios, instead of turning on the more costly DG1, ES was more frequently used with greater charge and discharge cycles to supply the load demand. The comparison between Figures 10 and 13 illustrates that the number of operation hours of the DG1 was significantly reduced. As illustrated in Figure 14, the greater reliance of the ES resulted in the higher S2S power demand to charge the ES. The power demand from the S2S was maximum at most time instances except for mid-day where there was additional support from the solar PV power generation. The demand response electricity price for this case study is also illustrated in Figure 14. As compared to Figure 11 in case study 1, the demand response electricity price was higher due to the higher power demand from the vessel. As the emphasis was to minimize the fuel consumption and operation cost minimization in the case study 2, the ES was much more frequently exploited. As a result, a higher number of charge and discharge cycles were being consumed as shown in Figure 15. Furthermore, the DOD and the number of operating hours for the ES are also significantly increased as compared to Figure 12. It is also observed that, the economic dispatch tried to charge the ES back to higher SOC whenever it was at the harbor for the upcoming operation tasks. In this study, the cost values of the objective functions 1 and 2 were 2.07×10^3 and 1.75×10^3. It also meant that the improvements of the objective function 1 and 2 were 44.8% and 2.78% improvement from their respective maxima values presented in Table 3. If the results are to be compared with the case study 1, it is observed that the operation cost, fuel, and emission efficiency improved from 28.25% to 44.78% which is close to the absolute optimality of the objective function 1. However, with regard to the ES degradation improvement, it only accounted for 2.78% improvement from its maximum value. Hence, the comparison between case study 1 and 2 has proven that such weight assignments will result in the unbalanced emphasis on the conflicting objective functions and the proposed method in this study has carefully developed a method to address such potential issues.

In this study, the optimization time horizon for the hour-ahead optimal scheduling remained at 24 h. In reality, to achieve a more accurate dispatch, the optimization horizon could be reduced to an hourly or half-day dispatch. With the updated prediction of the solar PV outputs, the objective weight sets could be updated accordingly based on the comparison study that was carried out in the first stage (day-ahead) scheduling. Hence, the proposed methods provided additional flexibility to the system operation of the vessel by providing a holistic representation of the dispatching scheme.

9. Conclusions

The study proposed the optimal scheduling of the ferry with the multi-objective functions. It addresses two conflicting objectives in the problem formulation; operation cost which accounts for fuel cost, CO_2 emission cost, grid charging cost, and maintenance cost while minimizing the degradation of the ES. The multi-objective optimization is solved with the proposed two-stage economic dispatch scheme. For the interval forecast data, Pareto-front solution spaces are mapped out to estimate the optimal sets of weight for the two objectives based on the user's preference due to the large difference in the numerical scale. Case studies with different sets of weights are illustrated to demonstrate the effectiveness of the proposed approach in the optimal scheduling of the ferry. The main conclusions from this research work are summarized as follows. (1) Due to the complexity of the model formulation and present of non-linear constraints, linearization of the constraints such as ES degradation can improve the computation efficiency to map-out the Pareto front solution space as well as to compute the hour-ahead dispatch. The simulation times are within seconds and hence the applicability of the proposed method for actual implementation can be assured. (2) The proposed method addresses the uncertainty present in the solar PV forecasting by mapping out the Pareto front solution space for the boundary conditions of the solar PV generation to have a better understanding of the solution space shift for the decision making in hour-ahead scheduling. The simulation results indicate that the higher penetration of solar PV will result in the higher Pareto front shift. Without understanding the solution space, optimal dispatch of the ES and generation sources can not be assured. (3) The results also indicated that with the proper ES management, the DOD of the ES can be effectively controlled by the vessel operator by adjusting the weight set points for the objective functions. From the observation of the average rate of change of energy in ES in Figure 8, the vessel operator can set the ramp rate limit of the ES to ensure the safe operation of the ES. Similar, fuel consumption and operation cost optimization can be done simultaneously with the proper sets of weight assignment for the objective functions. (4) The results also clearly indicate the influence of demand response grid electricity pricing scheme and the amount of solar PV generation on the power exchange with the S2S power supply. It is also observed that ESs are mainly charged from the grid especially when the grid electricity prices are lower. (5) The proposed two-stage multi-objective optimization method improve the accuracy of the generation dispatch result by employing higher time-resolution optimization only when the uncertainty is realized in the hour-ahead scheduling. In the future, more efforts can be spent on integrating more objectives such as thermal performance of the ES in the optimization framework.

Author Contributions: Conceptualization, K.H., X.Y. and G.W.; formal analysis, K.H., X.Y. and G.W.; investigation, K.H., X.Y. and G.W.; methodology, K.H., X.Y. and G.W.; validation, K.H., X.Y. and G.W.; visualization, X.Y. and G.W.; writing—original draft, K.H., X.Y. and G.W.; writing—review and editing, K.H., X.Y. and G.W. All authors have read and agreed to the published version of the manuscript.

Funding: This research received no external funding. The APC for this paper is waived by the guest editor.

Conflicts of Interest: The authors declare no conflict of interest.

Abbreviations

The following abbreviations are used in this manuscript:

Min/max	Minimum and Maximum Values
rated	Rated value
t	tth time step
T	Optimization time horizon (h)
Δt	Time step size (min)
ES/ESS	Energy Storage System
DGs	Diesel Generators
S2S	Shore-to-ship power supply

The following input parameters are used in this manuscript:

A_{PV}	Total installed area of the PV modules (m^2)
a_n, b_n, c_n	nth DG's fuel consumption coefficient
a_1, b_1, a_2, b_2	Curve fitting coefficients
α_0, α_1	Exponential Curve fitting coefficients
c_{P1}, c_{P2}	Propulsion power and speed correlation coefficient, and hull-dependent coefficient
$E_{ESS,rated}$	Rated ES Size (kWh)
F_{fuel}	Cost of diesel fuel ($/L)
F_{trans}	State transition cost of DGs ($/transition)
$F_{DG/PV,mai}$	Maintenance cost of DGs and PV ($/kW)
F_{co2}	Carbon credit cost per unit mass ($/kg)
f_{TOU}	Time of use electricity price ($/kWh)
Irr_{PV}	Irradiation data (W/m^2)
I_{ESS}	Investment cost of ES ($/kWh)
N	Number of DGs
N_{DOD}	Number of half cycles allowed for ES at a given depth of discharge
N_{static}	Total number of half cycles lost from static degradation of ES
N_{ave}	Average cycle used per year for ES
$N_{i,j}$	Normalized Solution Vector
$OM_{ESS/PV}$	Operation and maintenance cost ($/kWh)
$P^n_{ramp,\max}$	Ramp rate limits of n_{th} DG (kW/Δt)
P_{Prop}	Propulsion power requirement of ferry (kW)
P_{load}	Ferry Load Profile (kW)
P_{PV}	Solar power generation (kW)
r	Interest rate (%)
Sl	Salvage cost ($)
$S_{ESS,rated}$	Investment cost of ES ($)
$t^{N,\min on/off}_{DG}$	Minimum on/off time of the DG (minutes)
v	Velocity of the ferry (knots)
w_i	Weighted coefficient of the objective i
η	Efficiency (%)
ζ	Scaling factor of grid electricity price

The following variables are used in this manuscript:

cost_{fuel}	Total fuel consumption cost ($)
$\text{cost}_{SC/SD}$	Total startup and shutdown cost of DGs ($)
cost^{DG}_{mai}	Total maintenance cost of the DGs ($)
cost^{PV}_{mai}	Total maintenance cost of the PV ($)
cost_{grid}	Total cost of charging from grid ($)
$\text{cost}_{emission}$	Total cost of carbon tax for emission ($)
$\text{cost}_{ESS,deg}$	Total cost of ES degradation ($)
FC^n_{DG}	Fuel Consumption of nth DG (liter/kW)
F_{ele}	Demand response electricity price ($/kWh)
$f_{i,j}$	Objective function j in ith solution set ($)
P^n_{DG}	Output power of nth DG (kW)
P_{grid}	Power supplied from the grid (kW)
$P_{ch/dis}$	Charge and discharge power from ES (kW)
SOC	State of Charge of ES (%)
$t_{lt,ESS}$	Lifetime of ES (years)
u^n_{DG}	Binary on/off status of the DG
$u^n_{DG}(t_{on/off})$	State transition time instance on to off
$u^n_{DG}(t_{off/on})$	State transition time instance off to on
γ_s	Static degradation of ES
γ_d	Dynamic degradation of ES
γ_{acc}	Accumulated degradation of ES

References

1. International Maritime Organization. *Third IMO GHG Study 2014 Executive Summary and Final Reports*; International Maritime Organization: London, UK, 2015.
2. European Commission. *EU Strategy for Liquefied Natural Gas and Gas Storage*; European Commission: Brussels, Belgium, 2016.
3. International Maritime Organization. *Prevention of Air Pollution from Ships MARPOL ANNEX VL*; International Maritime Organization: London, UK, 1997.
4. International Maritime Organization. *Energy Efficiency Measures—Amendments MARPOL ANNEX VL*; International Maritime Organization: London, UK, 2013.
5. European Commission. *Roadmap to a Single European Transport Area—Towards a Competitive and Resource Efficient Transport System*; European Commission: Brussels, Belgium, 2011.
6. Corvus Energy. World's First All-Electric Car Ferry—Vessels and Shore Charging Stations. Available online: https://corvusenergy.com/ (accessed on 5 April 2020).
7. Koller, M.; Borsche, T.; Ulbig, A.; Andersson, G. Defining a degradation cost function for optimal control of a battery energy storage system. In Proceedings of the 2013 IEEE Grenoble Conference, Grenoble, France, 16-20 June 2013; pp. 1–6.
8. Perez, A.; Moreno, R.; Moreira, R.; Orchard, M.; Strbac, G. Effect of Battery Degradation on Multi-Service Portfolios of Energy Storage. *IEEE Trans. Sustain. Energy* **2016**, *7*, 1718–1729. [CrossRef]
9. Abdulla, K.; De Hoog, J.; Muenzel, V.; Suits, F.; Steer, K.; Wirth, A.; Halgamuge, S. Optimal Operation of Energy Storage Systems Considering Forecasts and Battery Degradation. *IEEE Trans. Smart Grid* **2018**, *9*, 2086–2096. [CrossRef]
10. Ju, C.; Wang, P.; Goel, L.; Xu, Y. A two-layer energy management system for microgrid with hybrid energy storage considering degradation costs. *IEEE Trans. Smart Grid* **2018**, *9*, 6047–6057. [CrossRef]
11. Kumar, J.; Kumpulainen, L.; Kauhaniemi, K. Technical design aspects of harbour area grid for shore to ship power: State of the art and future solutions. *Int. J. Electr. Power Energy Syst.* **2019**, *104*, 840–852. [CrossRef]
12. Sciberras, EA.; Zahawi, B.; Atkinson, D.J. Reducing shipboard emissions—Assessment of the role of electrical technologies. *Transp. Res. Part D Transp. Environ.* **2017**; *51*, 227–239. [CrossRef]
13. Kanellos, F.D.; Prousalidis, J.M.; Tsekouras, G.J. Control system for fuel consumption minimization-gas emission limitation of full electric propulsion ship power systems. *Proc. Inst. Mech. Eng. Part M J. Eng. Marit. Environ.* **2014**, *228*, 17–28. [CrossRef]
14. Shang, C.; Srinivasan, D.; Reindl, T. Economic and Environmental Generation and Voyage Scheduling of All-Electric Ships. *IEEE Trans. Power Syst.* **2016** *31*, 4087–4096. [CrossRef]
15. Boveri, A.; Silvestro, F.; Molinas, M.; Skjong, E. Optimal Sizing of Energy Storage Systems for Shipboard Applications. *IEEE Trans. Energy Convers.* **2018**, *34*, 801–811. [CrossRef]
16. Yao, C.; Chen, M.; Hong, Y.Y. Novel Adaptive Multi-Clustering Algorithm-Based Optimal ESS Sizing in Ship Power System Considering Uncertainty. *IEEE Trans. Power Syst.* **2018** *33*, 307–316. [CrossRef]
17. Shang, C.; Srinivasan, D.; Reindl, T. NSGA-II for joint generation and voyage scheduling of an all-electric ship. In Proceedings of the 2016 IEEE Congress on Evolutionary Computation (CEC), Vancouver, BC, Canada, 24–29 July 2016.
18. Jaurola, M.; Hedin, A.; Tikkanen, S.; Huhtala, K. Optimising design and power management in energy-efficient marine vessel power systems: A literature review. *J. Mar. Eng. Technol.* **2018**, *18*, 92–101. [CrossRef]
19. Kanellos, F.; Anvari-Moghaddam, A.; Guerrero, J. Smart Shipboard Power System Operation and Management. *Inventions* **2016**, *18*, 92–101. [CrossRef]
20. Hein, K.; Xu, Y. Hybrid Energy Storage System in Naval Vessel with 2-Stage Power-sharing Algorithm. In Proceedings of the 2019 IEEE Innovative Smart Grid Technologies—Asia (ISGT Asia), Chengdu, China, 21–24 May 2019; pp. 3607–3612.
21. Kanellos, F.D. Optimal power management with GHG emissions limitation in all-electric ship power systems comprising energy storage systems. *IEEE Trans. Power Syst.* **2014**, *29*, 330–339. [CrossRef]
22. Al-Falahi, M.D.A.; Nimma, K.S.; Jayasinghe, S.D.G.; Enshaei, H.; Guerrero, J.M. Power management optimization of hybrid power systems in electric ferries. *Energy Convers. Manag.* **2018**, *172*, 50–66. [CrossRef]
23. Wen, S.; Lan, H.; Hong, Y.Y.; Yu, D.C.; Zhang, L.; Cheng, P. Allocation of ESS by interval optimization method considering impact of ship swinging on hybrid PV/diesel ship power system. *Appl. Energy* **2016**, *175*, 158–167. [CrossRef]

24. Kanellos, F.D.; Tsekouras, G.J.; Hatziargyriou, N.D. Optimal demand-side management and power generation scheduling in an all-electric ship. *IEEE Trans. Sustain. Energy* **2014**, *5*, 1166–1175. [CrossRef]
25. Huang, Y.; Lan, H.; Hong, Y.Y.; Wen, S.; Fang, S. Joint voyage scheduling and economic dispatch for all-electric ships with virtual energy storage systems. *Energy* **2020**, *190*, 116268. [CrossRef]
26. Zhengmao, L.; Yan, X.; Sidun, F.; Yu, W. Multi-objective Coordinated Energy Dispatch and Voyage Scheduling for a Multi-energy Cruising Ship. In Proceedings of the 2019 IEEE/IAS 55th Industrial and Commercial Power Systems Technical Conference (I&CPS), Calgary, AB, Canada, 5–8 May 2019; pp. 1-8.
27. LithiumWerks. Lithium Phosphate Battery. Available online: https://lithiumwerks.com/technology/ (accessed on 5 April 2020).
28. Miner, M.A. Cumulative damage in fatigue *J. Appl. Mech.* **1945**, *12*, 159–164.
29. Energy Market Authority. Renewable Energy: Solar Generation Profile. Available online: https://www.ema.gov.sg/Renewable_Energy.aspx (accessed on 5 April 2020).
30. Lofberg, J. YALMIP: A toolbox for modeling and optimization in MATLAB. In Proceedings of the 2004 IEEE International Conference on Robotics and Automation (IEEE Cat. No.04CH37508), New Orleans, LA, USA, 2–4 September 2004; pp. 284–289.
31. Studio-CPLEX, IBM ILOG CPLEX Optimization. User's Manual-Version 12. Available online: https://www.ibm.com/ (accessed on 5 April 2020).
32. MQ Power. 500 kW Diesel on-Site Power Industrial Generator. Available online: http://www.powertechengines.com/MQP-DataSheets/ (accessed on 5 April 2020).
33. Cummins. Triton Power TP-C500-T1-60. Available online: https://www.americasgenerators.com/ (accessed on 5 April 2020).
34. Lai, C.S.; McCulloch, M.D. Levelized cost of electricity for solar photovoltaic and electrical energy storage. *Appl. Energy* **2017**, *150*, 191–203. [CrossRef]